Reproductive Toxicology 137 (2025) 109033

Contents lists available at ScienceDirect

Reproductive Toxicology

journal homepage: www.elsevier.com/locate/reprotox

Role of adipose-derived stem cell exosomes in paclitaxel-induced acute ovarian injury: An experimental approach

Betul Yalcın [a,*], Tugce K. Kalkan [b], Zeynep B. Gonen [c,d], Eda Koseoglu [e], Gozde O. Onder [d,e], Nur S. Gokdemir [d], Munevver Baran [f], Arzu Yay [d,e]

[a] Department of Histology and Embryology, Faculty of Medicine, Adıyaman University, Adıyaman, Turkey
[b] Department of Histology and Embryology, Faculty of Medicine, Kırşehir Ahi Evran University, Kırşehir, Turkey
[c] Department of Oral and Maxillofacial Surgery, Faculty of Dentistry, Erciyes University, Kayseri, Turkey
[d] Genome and Stem Cell Center (GENKOK), Erciyes University, Kayseri, Turkey
[e] Department of Histology and Embryology, Faculty of Medicine, Erciyes University, Kayseri, Turkey
[f] Department of Pharmaceutical Basic Science, Faculty of Pharmacy, Erciyes University, Kayseri, Turkey

ARTICLE INFO

Keywords:
Paclitaxel
Exosome
Angiogenesis
Inflammation

ABSTRACT

Paclitaxel (PTL) is commonly used in cancer therapy at varying doses and durations, often in combination with other chemotherapeutic agents. However, achieving therapeutic efficacy typically requires high doses, which are associated with considerable toxicity. Adipose-derived stem cells have shown therapeutic potential, particularly through the release of extracellular vesicles known as exosomes. This study investigated the potential protective effects of exosomes derived from adipose-derived mesenchymal stem cells (AMSC-Exos) in a rat model of PTL-induced acute ovarian injury. Twenty-eight rats were assigned to groups: control, PTL (7.5 mg/kg), AMSC-Exos (1×10^6 exosomes), and PTL+AMSC-Exos (7.5 mg/kg PTL + 1×10^6 exosomes). Three days after the administration, ovarian tissues were harvested for histological and biochemical analysis. Hematoxylin and eosin (H&E) and Masson's Trichrome (MT) staining revealed significant histopathological deterioration in the cortex and medulla of ovarian tissue in the PTL group compared to the PTL+AMSC-Exos group. Exosome treatment following PTL administration resulted in upregulation of VEGF and downregulation of HIF-1α, NF_KB-p65, and IL-1β immunostaining intensities. Additionally, AMH immunostaining intensity was increased in primary, preantral, and secondary follicles. Levels of TNF-α, IL-1β, and IL-6 were significantly lower in the exosome treated group than in the PTL group, according to the results of the ELISA. These findings demonstrate that AMSC-Exos exhibited beneficial effects against PTL-induced acute ovarian damage by reducing histopathological alterations, inflammation, and HIF-1α expression, while enhancing VEGF expression and ovarian reserve. AMSC-Exos may represent a promising therapeutic approach for preventing chemotherapy-induced ovarian toxicity.

1. Introduction

By 2040, the number of cancer cases is estimated to reach 28.4 million, while by 2025, approximately 100 million women worldwide are expected to be at risk of ovarian damage due to chemotherapy [1,2]. Therefore, elucidating the molecular mechanisms of chemotherapy-induced ovarian damage and developing effective strategies to protect the reproductive system are of critical importance. The ovary is an essential organ with a fundamental role in fertility and endocrine balance. It is susceptible to chemotherapy, a vital treatment for cancer [3]. Chemotherapy is associated with several adverse outcomes, including dysregulation of ovarian hormones, amenorrhea, premature ovarian insufficiency (POI), and subsequent infertility [4,5]. One of these chemotherapeutics, PTL, approved by the FDA as the first chemotherapeutic agent sourced from a plant, is derived from the taxus plant [6,7]. PTL is widely utilized in clinical practice, often in combination with other gonadotoxic drugs. Initially, some clinical studies suggested that PTL did not have a negative impact on ovarian function. However, subsequent studies demonstrated that it reduces ovarian reserve and causes significant ovarian toxicity in premenopausal women [8]. PTL treatment has also been reported to exert adverse effects, including vascular structural damage, reduced blood flow [9,10], and

* Corresponding author at: Department of Histology and Embryology, Adıyaman University, Faculty of Medicine, Adıyaman 02040, Turkey.
E-mail address: byalcin@adiyaman.edu.tr (B. Yalcın).

https://doi.org/10.1016/j.reprotox.2025.109033
Received 1 July 2025; Received in revised form 29 July 2025; Accepted 13 August 2025
Available online 18 August 2025

depletion of the ovarian follicle pool [11,12]; however, the existing literature on this subject remains insufficient [3].

The capacity of mesenchymal stem cells to repair damage has recently attracted significant attention. The cells, widely distributed throughout the body, including the umbilical cord, bone marrow, fat, and amniotic membrane, are reported to provide protection against premature ovarian failure (POF) resulting from chemotherapy [13]. Concurrently, the exosome formed by these cells contributes to intercellular communication by binding to the receptor in the target cell with a diameter of 40–150 nm [14,15]. The functions of exosomes are mediated by DNA, various types of RNA (including circular and messenger RNAs), as well as proteins and lipids [16]. Following POF, exosome treatment leads to an enhancement in follicle number, recovery of hormone levels, an increase in ovarian granule cells' proliferation rate, and a decrease in their apoptosis rate [17]. In this study, adipose-derived mesenchymal stem cells (AMSCs) were selected as the preferred source of exosomes due to their ease of isolation from adipose tissue [18], high stem cell density, and favorable volumetric properties [19]. AMSC-Exos have the potential to promote ovarian function and may represent a novel, safe, and effective therapeutic strategy for preventing POI and enhancing female reproductive health [17].

AMSC-Exos have been identified as potential inducers of angiogenesis in endothelial cells, with the mechanism involving the secretion of growth factors via angiogenesis-related microRNAs [20]. Taxanes, known to inhibit mitotic activity, have been shown to suppress angiogenesis [21]. Angiogenesis is implicated in a variety of physiological processes, including human folliculogenesis, ovulation, and corpus luteum formation [22,23]. Ovarian angiogenesis is essential for follicular maintenance, and its disruption, whether due to endothelial cell damage or insufficient capillary network formation, may lead to follicular atresia or degeneration [24]. Moreover, the ovarian stroma is affected by it due to the dense network of blood vessels, which facilitate the efficient supply of nutrients to growing follicles, supporting their development and function [25]. For these reasons, this study aimed to assess the effects of AMSC-Exos on the ovary following PTL treatment, a chemotherapeutic agent currently utilized both as monotherapy and in combination with other agents in cancer treatment protocols.

2. Materials and methods

2.1. Animals

The present study employed a total of 28 female Wistar albino rats aged 16–24 weeks. The present study was conducted in accordance with the approval granted by the Erciyes University Animal Research Ethics Committee for the use of experimental animals (Approval No: 2022–22/066). The allocation of animals and the execution of the experimental procedures were carried out at the Erciyes University Experimental Research and Application Center. The subjects were accommodated in a standardized condition, with a temperature of 23 ± 2°C, within a period of 12 h of light/dark. The food and water requirements of the rats placed in experimental animal cages were met on an ad libitum basis.

2.2. Isolation and characterization of AMSCs and AMSC-Exos

Human AMSCs (hAMSCs) were provided by the Erciyes University Genome and Stem Cell Center. Following thawing at 37°C in a water bath, AMSCs were cultured in α-Modified Eagle's Medium (α-MEM) supplemented with 1 % antibiotics, 1 % stable L-glutamine, and 10 % fetal bovine serum (FBS). To facilitate exosome release, the culture medium was replaced with an FBS-free medium 24 h prior to secretome collection. Exosome isolation was performed using a commercial precipitation-based solution (ExoQuick-TC, System Biosciences).

For structural characterization, hAMSC-Exos morphology was assessed via scanning electron microscopy (SEM), and the size distribution of MSC-derived exosomes was further analyzed using a Nanoparticle Tracking Analysis (NTA) system. Exosomes isolated from hAMSCs were imaged using SEM (Zeiss GEMINI 500, Almanya) at the Erciyes University Technology Research and Application Center. A 30 μL volume of exosome resuspension from hAMSCs was carefully applied onto a sterile slide and evenly spread using a pipette. The slides were allowed to dry at room temperature, then coated with gold-palladium and prepared for SEM imaging. The diameter of the exosomes was measured in ten different areas of the images obtained using the ImageJ program, and the mean exosome size was calculated.

The size of exosomes, a key parameter in their characterization, was determined using an NTA system (Malvern Instrument Nanosight NS300, UK) at Erciyes University's Nanotechnology Research Center. The final volume of hAMSC-Exos was adjusted to 1 mL using DPBS. The measurement of hAMSC-Exos was performed using an instrument optimized according to the manufacturer's software guidelines (NanoSight NS300 Kullanıcı Kılavuzu, MAN0541-01-TR-00, 2017).

2.3. Experimental protocol

Rats were weighed, and those with comparable weights were assigned to the same experimental group. The quantity of PTL to be delivered to each subject was guided by reference to the findings of precedent studies [26,27].

In this study, four groups were formed, with each group comprising seven rats.

The rats in Group 1 (control group) were not administered any treatment.

The rats in Group 2 (PTL group) were administered 7.5 mg/kg intraperitoneally as a single dose [26,28].

In the rats in Group 3 (AMSC-Exos group (AMSC-Exos)), 1×10^6 exosomes were administered intravenously [29, 17].

In the rats in Group 4 (PTL and AMSC-Exos group (PTL+AMSC-Exos)), 7.5 mg/kg was administered intraperitoneally, and 1×10^6 exosomes intravenously.

Three days following the final administration, the rats were euthanized by cervical dislocation under xylazine and ketamine anesthesia (10 mg/kg and 60 mg/kg, intraperitoneally). Upon termination of the experimental procedure, the ovaries from all groups were retrieved for further examination via histological, immunohistochemical, and biochemical studies. The left ovaries were exposed to a 10 % formaldehyde solution for histological analysis, while the right ovaries were maintained at −80 °C for biochemical analysis.

2.4. Histopathological observations

After formaldehyde fixation, ovarian tissues were subjected to a series of histological procedures to prepare them for paraffin embedding. Initially, excess fixative was removed by rinsing with water, after which ovarian tissues were dehydrated through a graded ethanol series. Subsequently, clearing with xylene and embedding in paraffin were performed. The 5 μm sections prepared from the paraffin blocks were subjected to staining with H&E and MT. An Olympus BX51 light microscope (Japan), equipped with a camera, was utilized for the examination of the preparations and the acquisition of images. In order to detect ovarian damage, twenty non-overlapping fields were randomly selected at 40x magnification from each rat and the mean values for each group were subsequently evaluated. Ovarian scoring was conducted in accordance with the criteria for vascular congestion, hemorrhage, follicular degeneration, and fibrosis. In order to assess the severity of the histopathological damage in the ovarian tissue section, a scoring system that adopted the specified criteria was employed, with scores ranging from 0 to 3 [30,31].

2.5. Immunohistochemistry

The ovarian sections underwent a process of deparaffination,

hydration, and an incubation in distilled water. They were treated with citrate buffer (0.01 M, pH 6.0) at 95 °C for 10 min, followed by incubation in the same buffer at room temperature for an additional 10 min. Termination of the hydrogen peroxide activity was achieved by utilising 3 % H_2O_2 for 10 min., and then ultra-V block incubation was completed for 10 min. AMH (1:200, Sc166752, Santa Cruz, Oregon, USA), NF_KB-p65 (1:300, D14E12, Cell Signaling), VEGF (1:200, Sc152, Santa Cruz, Oregon, USA), IL-1β (1:50, BT-AP04469, Bioassay Technology Laboratory, Zhejiang, China), HIF-1α (1:400, Sc535446, Santa Cruz, Oregon, USA), and PCNA (1:400, Sc9857, Santa Cruz, Oregon, USA) primer antibodies were dripped onto the circled sections. After being incubated with primer antibodies during the night at 4°C, they were treated with biotinylated secondary antibody (goat anti-rabbit) and avidin-biotin-peroxidase for 10 min. For all other steps, PBS washing was performed with the exception of UV blocking. The brown-stained areas created by the peroxidase activity became visible after 3,3′-diaminobenzidine treatment and their nuclear staining was performed with hematoxylin. Following the staining procedure, the sections were treated with increasing concentrations of alcohol and xylene, with the aim of coating them with Entellan.

For each primary antibody, a total of ten images were obtained for each of the seven rats in each group using an Olympus BX51 microscope. The mean intensity of immunostaining was obtained from the images by way of the ImageJ program (NIH, USA) Onder et al. [32].

2.6. Enzyme-linked immunosorbent assay

Levels of tumor necrosis factor-alpha (TNF-α), interleukin 6 (IL-6), and interleukin 1β (IL-1β) were determined using Rat TNF-α (Sunred Bio, 201–11–0765, Shanghai, China), Rat IL-6 (Sunred Bio, 201–11–0136, Shanghai, China), and Rat IL-1β (Sunred Bio, 201–11–0120, Shanghai, China) enzyme-linked immunosorbent assay (ELISA) kits, using the manufacturers' instructions as a guide.

Initially, the homogenization process was applied to ovarian tissues stored at −80°C, utilizing phosphate buffer (pH 7.4, 20 mM). The supernatant was obtained from the homogenates by centrifugation at +4°C, 5000×g for 15 min. The standard wells were filled with 50 μl of varying concentrations of standards, prepared from the standard solution. The sample wells were filled with 40 μl of sample and 10 μl of antibody. After the HRP treatment at 37 °C for 60 min, the microplate was washed in wash buffer five times. Then, 50 μl of chromogen A and chromogen B were applied separately at 37 °C for 10 min, respectively. After the addition of the stop buffer, absorbance was measured at a wavelength of 450 nm using a microplate reader, and protein concentration was expressed in picograms per milligram [33].

2.7. Statistical analysis

The Shapiro-Wilk and Kolmogorov-Smirnov tests were performed to assess the normality of the data. If the data were normally distributed, one-way analysis of variance (ANOVA) followed by Tukey's post hoc test was used to compare quantitative variables. For histopathological scoring data that were not normally distributed, Dunn's multiple comparison test was applied. A p-value of less than 0.05 was considered statistically significant. The statistical analyses were performed using GraphPad Prism software (version 9.0).

3. Results

3.1. Characterization of AMSC-Exos

The size of AMSC-Exos was determined using an NTA system, revealing a size distribution of 129.5 ± 47.4 nm (Fig. 1A). Additionally, exosome morphology, another key characteristic, was analyzed using SEM, demonstrating a spherical shape with an average size of 116.2 ± 12.1 nm (Fig. 1B).

3.2. Histopathological alterations of ovarian tissues

Under light microscopy, the histopathological effects of PTL on ovarian morphology were assessed using H&E staining. In the control group, ovarian tissue exhibited well-preserved histoarchitecture, including a cortex with developing follicles and a medulla composed of loose connective tissue. Similarly, the ovarian tissue in the AMSC-Exos only group displayed a histological appearance comparable to that of the control group. In contrast, the PTL-only group exhibited disrupted follicular structures, edema, dilated or congested blood vessels in the medulla, indicating significant alterations in tissue architecture. The alterations observed in the PTL group were less pronounced in the AMSC-Exos treatment group, and based on histopathological scoring, this improvement was statistically significant (Fig. 2 and Table 1).

To evaluate potential changes in the ovarian connective tissue, MT staining was performed. In the ovarian cortex of the control group, thin tunica albuginea was observed beneath the germinal epithelium and cortical connective tissue septa were identified. Additionally, thin collagen fibers were present in the perivascular regions of the ovarian medulla, an area characterized by its abundance of blood vessels. In contrast, the PTL group exhibited thickening of the cortical connective tissue septa, as well as an increased density of collagen fibers extending from the medulla to the cortex and surrounding the blood vessels. The administration of PTL in conjunction with AMSC-Exos therapy resulted in a decline in collagen fiber abundance within the cortex and medulla (Fig. 2 and Table 1).

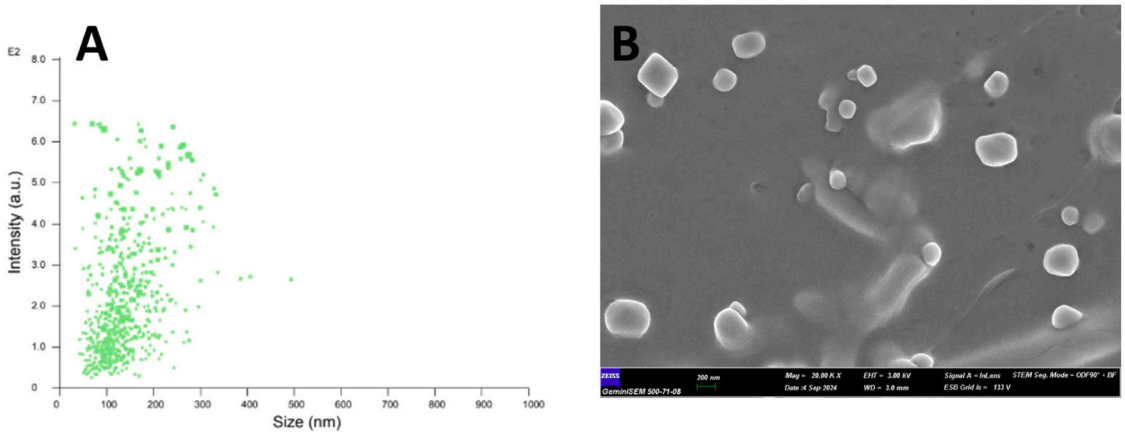

Fig. 1. Characterization of AMSC-Exos. A. Size distributions of AMSC-Exos by NTA. B. Transmission electron microscopy image of AMSC-Exos, scale bar = 200 nm.

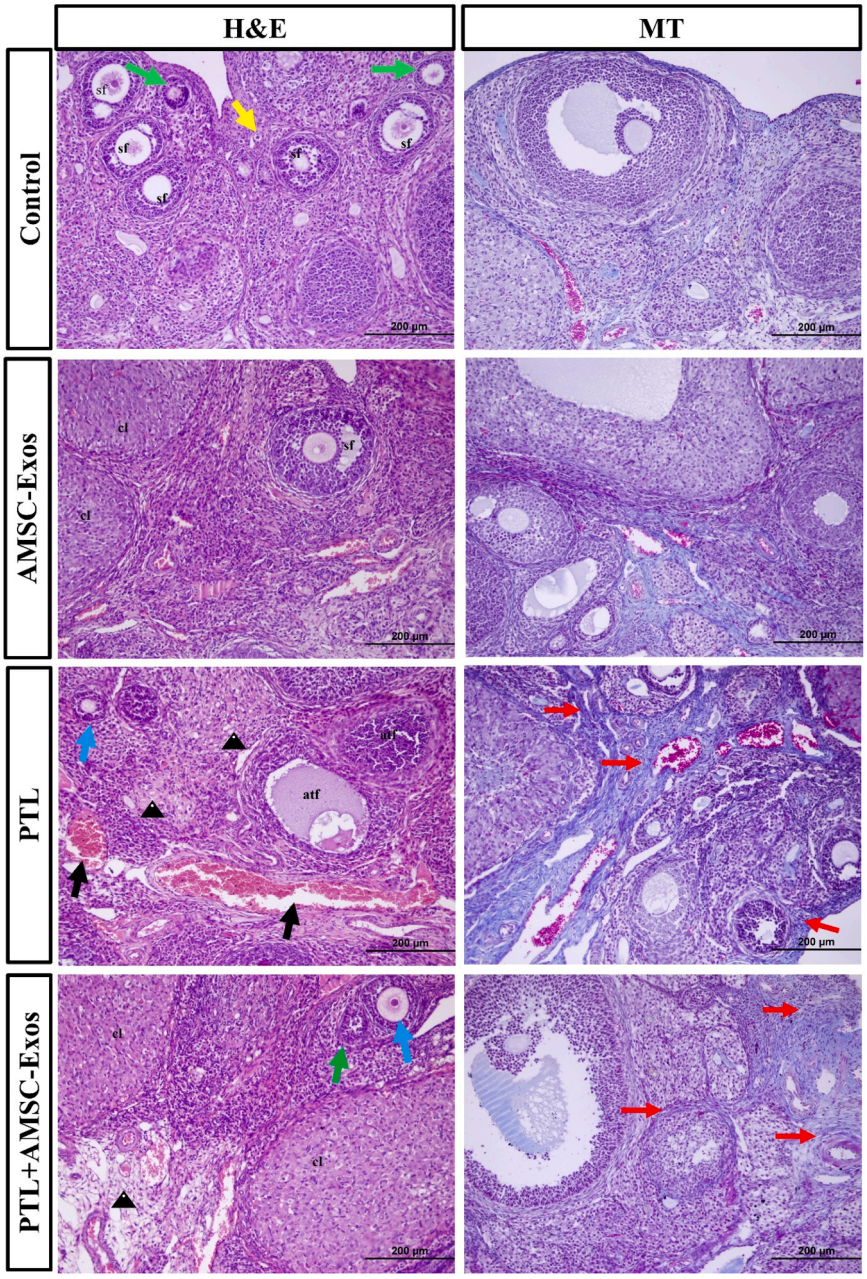

Fig. 2. H&E and MT staining of rat ovarian tissues. Primordial follicles (yellow arrow), primary follicles (green arrow), preantral follicle (blue arrow), secondary follicle (sf), corpora lutea (cl) and atretic follicles (atf). Congested blood vessels (black arrow), edema (arrowhead) and fibrosis (red arrow). Original magnification 20x; scale bar 200 µm. In H&E staining, the cortex of the control and AMSC-Exos groups exhibits the healthy follicles in different types; in contrast, the PTL group exhibited disrupted follicular structures. In PTL group medulla, edema and congested blood vessels were detected. AMSC-Exos therapy mitigated PTL-induced damage in follicular and medullary ovarian structures. In MT staining, the PTL group increased collagen fiber density in the perivascular regions and septa extending from the medulla to the cortex. The distribution and density of collagen fibers did not significantly increase in the other groups, in contrast to the PTL group.

Table 1
The results of statistical analyses of histopathological scoring.

	Control	AMSC-Exos	PTL	PTL+AMSC-Exos	p
Vascular Congestion	0.00(0.00–0.00)[a]	0.00(0.00–0.25)[a]	3.00(2.00–3.00)[b]	0.00(0.00–1.25)[a]	<0.0001
Hemorrhage	0.00(0.00–0.00)[a]	0.00(0.00–0.00)[a]	2.00(2.00–2.00)[b]	0.00(0.00–0.00)[a]	<0.0001
Follicle Degeneration	0.00(0.00–0.00)[a]	0.00(0.00–0.25)[a]	3.00(2.00–3.00)[b]	0.00(0.00–1.25)[a]	<0.0001
Fibrosis	0.00(0.00–0.00)[a]	0.00(0.00–0.00)[a]	3.00(2.00–3.00)[b]	0.00(0.00–0.25)[a]	<0.0001

Values are expressed as median (quarter 1-quarter 3); statistical comparisons are denoted by lettering, with shared letters indicating nonsignificant differences and distinct letters indicating significance.

3.3. Immunohistochemical findings

To provide further insight into the function of AMSC-Exos, immunohistochemistry was employed to assess VEGF and HIF-1α immunostaining intensity (Fig. 3). For VEGF, the immunostaining intensity was statistically similar across all groups, except for the PTL group, which showed a significant decrease. For HIF-1α, the immunostaining intensity was found to be significantly elevated in the AMSC-Exos and PTL+AMSC-Exos groups in comparison to the control group. The increase noted in the PTL group was also statistically significant compared to all other groups. However, compared to the PTL group, the PTL+AMSC-Exos group demonstrated a decrease (Table 2).

The intensity of NF_KB-p65 and IL-1β immunostaining was observed to be highest in the PTL group. For NF_KB-p65, a significant difference was observed between the PTL group and all other groups, while no significant difference was evident between the other groups. For IL-1β, a significant decrease in intensity was observed in the PTL+AMSC-Exos group when compared with the PTL group and a significant increase when compared with the AMSC-Exos group (Fig. 3 and Table 2).

AMH, a crucial marker of follicular development, was evaluated by immunohistochemistry, and its immunostaining intensity was measured. The presence of AMH immunostaining was observed in certain follicle types, specifically in granulosa cells of primary, preantral, and secondary follicles. Among all three follicle types, the PTL group exhibited the lowest immunostaining intensity, which was statistically significant compared to the other groups (Fig. 4 and Table 3).

3.4. Biochemical findings

In order to ascertain the anti-inflammatory effect of AMSC-Exos, the pro-inflammatory cytokines TNF-α, IL-1β, and IL-6 levels in ovarian tissues were measured by ELISA. Administration of PTL led to a significant ($p < 0.001$) increase in levels of TNF-α, IL-1β and IL-6. In the PTL+AMSC-Exos group, the levels of these cytokines were statistically decreased (Table 4). There was no significant difference between the other groups for TNF-α and IL-1β levels. For IL-6 levels, PTL+ AMSC-Exos group showed a statistically significant decrease compared to the PTL group, and a significant increase compared to the other groups.

Table 2
The results of statistical analyses of VEGF, HIF-1α, NFκB-p65, and IL-1β immunostaining intensities in all experimental groups.

	Control	AMSC-Exos	PTL	PTL+AMSC-Exos	p
VEGF	(88.26 ± 4.83)^{a}	(86.59 ± 5.15)^{a}	(79.08 ± 6.83)^{b}	(84.16 ± 5.71)^{a}	<0.0001
HIF−1α	(65.59 ± 5.22)^{a}	(77.67 ± 11.88)^{b}	(92.29 ± 9.20)^{c}	(83.73 ± 6.03)^{b}	<0.0001
NF_KB-p65	(82.70 ± 6.68)^{a}	(84.54 ± 7.10)^{a}	(90.68 ± 5.10)^{b}	(84.29 ± 5.63)^{a}	<0.0001
IL−1β	(76.33 ± 7.46)^{ac}	(73.78 ± 4.68)^{a}	(87.51 ± 5.39)^{b}	(80.36 ± 4.98)^{c}	<0.0001

Values are expressed as mean ± standard deviation; statistical comparisons are denoted by lettering, with shared letters indicating nonsignificant differences and distinct letters indicating significance.

4. Discussion

The present study demonstrated that acute PTL administration induces ovarian damage, which can be effectively alleviated by AMSC-Exos. Histopathological analysis revealed that PTL treatment resulted in the disruption of follicular structures, edema, dilatation or occlusion

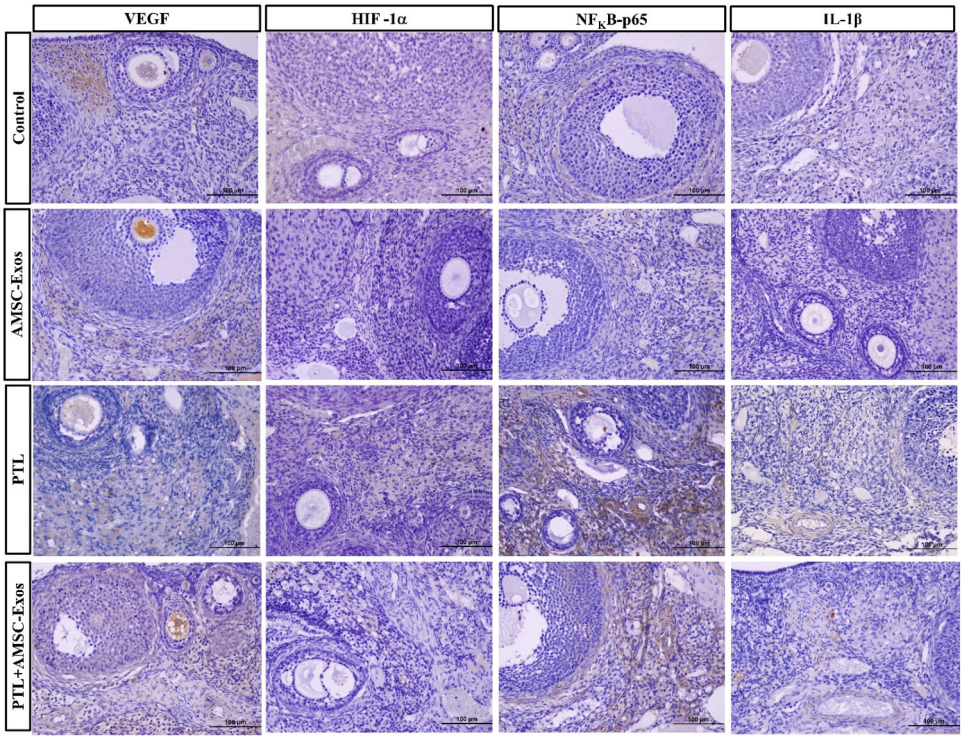

Fig. 3. Effect of AMSC-Exos on VEGF, HIF-1α, NF_KB-p65 and IL-1β immunostaining in rat ovarian sections from each experimental group. Representative images of VEGF, HIF-1α, NF_KB-p65 and IL-1β immunostaining at × 40 magnification (400 ×). Immunostaining of VEGF in the AMSC-Exos-treated group shows an intense cytoplasmic reaction in the cells, while the PTL group shows a mild immunostaining pattern. PTL+AMSC-Exos shows similar immunostaining except for the PTL group. HIF-1α immunostaining in the PTL group exhibits the highest cytoplasmic reactivity of stromal cells, whereas the PTL + AMSC-Exos group demonstrates a notable reduction in staining intensity. NFKB-p65 immunostaining in the PTL group exhibits the highest cytoplasmic and nuclear reactivity, which was statistically significant compared to the other groups. However, no significant differences were observed among the remaining groups. IL-1β immunostaining in the PTL group exhibits the highest cytoplasmic reactivity, whereas the PTL + AMSC-Exos group demonstrated reduced staining intensity.

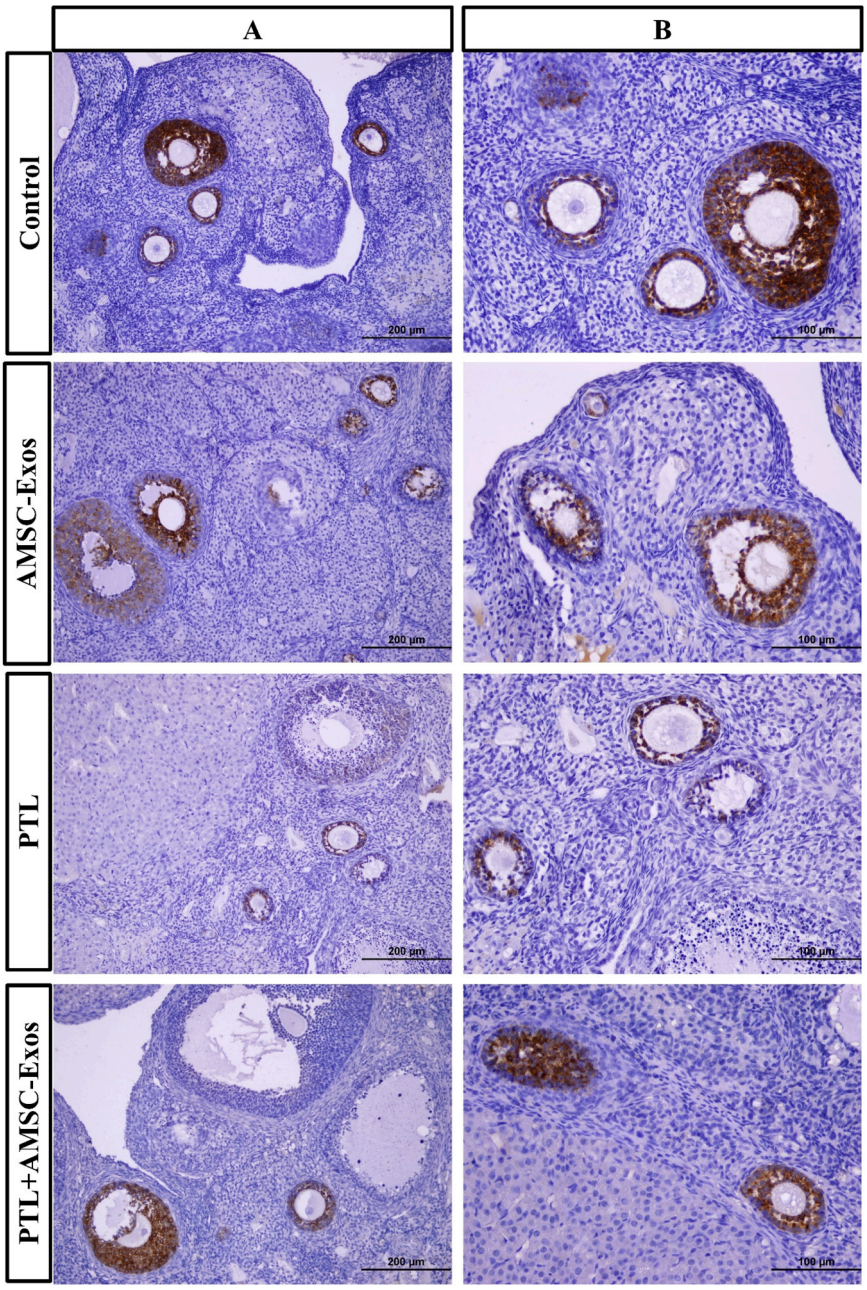

Fig. 4. Effect of AMSC-Exos on AMH immunostaining in rat ovarian sections from each experimental group. AMH immunostaining was predominantly observed in the cytoplasm of developing granulosa cells. (A) Representative images of AMH immunostaining at ×20 magnification (200×). (B) Representative images of AMH immunostaining at ×40 magnification (400 ×). For all types of primary, preantral, and secondary follicles, the PTL group exhibited the lowest immunostaining intensity. Compared to the PTL group, the PTL + AMSC-Exos group exhibited a significantly higher staining intensity.

Table 3
The results of statistical analyses of AMH immunostaining intensities in primary, preantral, and secondary follicles of all experimental groups.

AMH	Control	AMSC-Exos	PTL	PTL+AMSC-Exos	p
Primer	(114.4 ± 21.24)^{a}	(117.9 ± 14.21)^{a}	(87.13 ± 9.68)^{b}	(108.3 ± 25.81)^{a}	0.0086
Preantral	(121.7 ± 11.05)^{a}	(119.6 ± 13.08)^{a}	(105.4 ± 9.12)^{b}	(121.2 ± 14.53)^{a}	0.0002
Sekonder	(113.3 ± 18.97)^{a}	(120.5 ± 14.87)^{a}	(89.06 ± 12.13)^{b}	(105.6 ± 13.19)^{a}	<0.0001

Values are expressed as mean ± standard deviation; statistical comparisons are denoted by lettering, with shared letters indicating nonsignificant differences and distinct letters indicating significance.

Table 4
ELISA results of statistical analyses of TNF-α, IL-1β and IL-6 levels in the ovaries of all experimental groups.

ELISA	Control	AMSC-Exos	PTL	PTL+AMSC-Exo	p
TNF-α	(137.1 ± 12.12)^{a}	(135.3 ± 18.34)^{a}	(166.4 ± 7.05)^{b}	(133.0 ± 12.28)^{a}	0.0101
IL−1β	(664.7 ± 125.2)^{a}	(686.7 ± 148.2)^{a}	(1025.0 ± 89.56)^{b}	(694.7 ± 136.5)^{a}	0.0046
IL−6	(29.32 ± 7.36)^{a}	(31.63 ± 2.84)^{a}	(67.79 ± 8.06)^{b}	(49.40 ± 5.13)^{c}	<0.0001

Values are expressed as mean ± standard deviation; statistical comparisons are denoted by lettering, with shared letters indicating nonsignificant differences and distinct letters indicating significance.

of blood vessels. However, the adverse effects of acute PTL-induced ovarian injury were prevented by AMSC-Exos, which exert protective effects on both ovarian tissue integrity and AMH levels. These protective effects are likely mediated through the attenuation of HIF-1α, NF_KB-p65, and pro-inflammatory cytokines, including TNF-α, IL-1β, and IL-6, within the ovarian tissue.

In the present study, a single acute dose of 7.5 mg/kg PTL was observed to induce marked alterations in both the general histopathological architecture and the fibrotic pattern of the ovary. Disruption of the follicular architecture within the cortex, along with congestion, dilatation, and edematous areas in the blood vessels of the medulla, were particularly prominent. MT staining revealed an accumulation of collagen fibers in both the connective tissue septa and around blood vessels in response to PTL treatment. However, treatment with a single dose of AMSC-Exos attenuated these PTL-induced alterations, accompanied by a concurrent decrease in collagen fiber. According to the findings of Elfayomy et al., the administration of 7.5 mg/kg PTL-induced ovarian shrinkage, cortical follicle depletion, and a significant decrease in antral follicle counts [34]. These detrimental changes are believed to result from the delayed meiotic maturation of oocytes, leading to the formation of aneuploid oocytes. The maintenance of ovarian development and function critically depends on angiogenesis [35]. In cases of POF, regulation of angiogenesis supports follicular growth and overall ovarian activity [36]. Exposure to a low dose of PTL limits the infiltration of bone marrow-derived endothelial progenitor cells into the tumor microenvironment and reduces microvessel density [37]. Exosomes released by AMSCs contain microRNAs (miRNAs) that promote angiogenesis and activate endothelial cells by stimulating the secretion of VEGF and epidermal growth factor [20]. Therefore, AMSC-Exos may contribute to the treatment of ovarian disorders [17]. Under hypoxic conditions, the regulation of VEGF is primarily mediated by HIF-1α, a key transcription factor. HIF-1α facilitates this process by promoting an increase in oxygen supply through the induction of angiogenesis [38]. Due to increased oxygen demand during follicular growth, ovarian hypoxia activates HIF-1, which in turn promotes VEGF-mediated angiogenesis [39,40]. The present study demonstrates that PTL leads to a decrease in VEGF and an increase in HIF-1α staining intensity; conversely, the combination of PTL and AMSC causes a reversal of these staining patterns. This effect may be associated with the ability of AMSC-derived exosomes to promote vascular endothelial cell functions, thereby enhancing angiogenesis [41].

One of the members of the TGF-β superfamily, AMH, is secreted by secondary and early antral follicle granulosa cells and serves as a reliable biomarker for assessing ovarian reserve following chemotherapy [42,43]. It has the ability to inhibit the maturation of growing follicles by preventing the activity of primordial follicles and reducing the sensitivity of antral follicles to FSH, thereby contributing to the preservation of the ovarian follicular pool [44]. In a study investigating, for the first time, the interaction between AMSC-Exos and POF, administration of AMSC-Exos successfully restored AMH expression levels to control values after in a cyclophosphamide-induced POF model [17]. The study further reported that it could potentially stimulate the restoration of primordial, primary, antral, and secondary follicles. In the current study, AMCS treatment significantly ameliorated the reduction in serum AMH levels, which may be attributed to the protective effect of AMSC intervention against PTL-induced ovarian damage, particularly in the follicular granulosa cells. NF-κB is an important molecule capable of activating enzymes and proinflammatory cytokines. Its activity can be triggered by growth factors, infectious agents, and chemotherapy drugs [45,46].

PTL-induced inflammatory damage in multiple tissues was characterised by enhanced activation of pro-inflammatory markers, such as NF-κB, TNF-α, IL-1β, IL-6, and iNOS [47]. In the ovary, beyond its role in promoting immune and inflammatory responses, this molecule also contributes to the regulation of granulosa cell function during folliculogenesis [48,49]. These findings may offer valuable insights into the underlying mechanisms responsible for the decline in follicular reserve observed in these females [50]. To the best of our knowledge, the effects of AMSC-Exos on PTL-induced acute ovarian damage have not previously been investigated. In our study, PTL administration significantly increased the levels of NF_KB-p65, TNF-α, IL-1β, and IL-6 in ovarian tissue compared to both the AMSC-Exos treated and control groups. The anti-inflammatory functions of mesenchymal stem cells and their exosomes are largely attributed to the inhibition of the TLR4/NF-κB [51]. Among them, AMSC-Exos significantly contribute to the regulation of immune function and the control of inflammation [52]. In conclusion, this study demonstrated that AMSC-Exos alleviated acute ovarian injury induced by PTL by activating the VEGF signaling pathway and inhibiting the pro-inflammatory response (TNF-α, IL-1β, and IL-6) as well as their key regulator, NF_KB-p65. Furthermore, AMSC-Exos treatment increased AMH immunostaining intensity, which was consistent with the marked improvements observed in follicular histology. Taken together, these results highlight the therapeutic potential of AMSC-Exos in preserving ovarian function and structure following PTL-induced injury.

Declaration of Competing Interest

The authors declare that they have no known competing financial interests or personal relationships that could have appeared to influence the work reported in this paper.

Data availability

Data will be made available on request.

References

[1] H. Sung, J. Ferlay, R.L. Siegel, M. Laversanne, I. Soerjomataram, A. Jemal, et al., Global cancer statistics 2020: GLOBOCAN estimates of incidence and mortality worldwide for 36 cancers in 185 countries, CA Cancer J. Clin. 71 (3) (2021), 209–49.
[2] B. Sun, J. Yeh, Onco-fertility and personalized testing for potential for loss of ovarian reserve in patients undergoing chemotherapy: proposed next steps for development of genetic testing to predict changes in ovarian reserve, Fertil. Res. Pract. 7 (1) (2021) 13.
[3] C. Wu, T. Wu, D. Chen, S. Wei, W. Tang, L. Xue, J. Xiong, Y. Huang, Y. Guo, Y. Chen, M. Wu, S. Wang, The effects and mechanism of taxanes on chemotherapy-associated ovarian damage: a review of current evidence, Front Endocrinol. (Lausanne) (2022) 13.
[4] W. van Dorp, R. Haupt, R.A. Anderson, R.L. Mulder, M.M. van den Heuvel-Eibrink, E. Van Dulmen-Den Broeder, H.I. Su, J.F. Winther, M.M. Hudson, J.M. Levine, W. H. Wallace, Reproductive function and outcomes in female survivors of childhood, adolescent, and young adult cancer: a review, J. Clin. Oncol. 36 (21) (2018) 2169–2180.
[5] N. Spears, F. Lopes, A. Stefansdottir, V. Rossi, M. De Felici, R.A. Anderson, F. G. Klinger, Ovarian damage from chemotherapy and current approaches to its protection, Hum. Reprod. Update 25 (6) (2019) 673–693.
[6] L. Zhu, L. Chen, Progress in research on paclitaxel and tumor immunotherapy, Cell Mol. Biol. Lett. 24 (2019) 40.
[7] Y.H. Yang, J.W. Mao, X.L. Tan, Research progress on the source, production, and anti-cancer mechanisms of paclitaxel, Chin. J. Nat. Med. 18 (12) (2020) 890–897.
[8] J.A. Petrek, M.J. Naughton, L.D. Case, E.D. Paskett, E.Z. Naftalis, S.E. Singletary, et al., Incidence, time course, and determinants of menstrual bleeding after breast cancer treatment: a prospective study, J. Clin. Oncol. 24 (7) (2006) 1045–1051.
[9] I. Ben-Aharon, I. Meizner, T. Granot, S. Uri, N. Hasky, S. Rizel, R. Yerushalmi, A. Sulkes, S.M. Stemmer, Chemotherapy-induced ovarian failure as a prototype for acute vascular toxicity, Oncologist 17 (11) (2012) 1386–1393.
[10] G. Bildik, N. Akin, F. Senbabaoglu, G.N. Sahin, S. Karahuseyinoglu, U. Ince, C. Taskiran, U. Selek, K. Yakin, Y. Guzel, et al., GnRH agonist leuprolide acetate does not confer any protection against ovarian damage induced by chemotherapy and radiation in vitro, Hum. Reprod. 30 (2015) 2912–2925.
[11] B. Ozcelik, C. Turkyilmaz, M.T. Ozgun, I.S. Serin, C. Batukan, S. Ozdamar, A. Ozturk, Prevention of paclitaxel and cisplatin induced ovarian damage in rats by a gonadotropin-releasing hormone agonist, Fertil. Steril. 93 (5) (2010) 1609–1614.
[12] M. Maidarti, W. Tarumi, S. Takae, B. Wiweko, N. Suzuki, Paclitaxel is evidence to reduce growing ovarian follicle growth in mice model study, Toxicol. Vitr. 83 (2022) 105386.
[13] Y.X. Fu, J. Ji, F. Shan, J. Li, R. Hu, Human mesenchymal stem cell treatment of premature ovarian failure: new challenges and opportunities, Stem Cell Res. Ther. 12 (1) (2021) 161.
[14] Z. Azari, S. Nazarnezhad, T.J. Webster, S.J. Hoseini, P. Brouki Milan, F. Baino, S. Kargozar, Stem cell-mediated angiogenesis in skin tissue engineering and wound healing, Wound Repair Regen. 30 (4) (2022) 421–435.

[15] Y. Tang, Y. Zhou, H.J. Li, Advances in mesenchymal stem cell exosomes: a review, Stem Cell Res. Ther. 12 (1) (2021) 71.
[16] L. Barile, G. Vassalli, Exosomes: therapy delivery tools and biomarkers of diseases, Pharm. Ther. 174 (2017) 63–78.
[17] B. Huang, J. Lu, C. Ding, Q. Zou, W. Wang, H. Li, Exosomes from human adipose mesenchymal stem cells improve ovary function of premature ovarian insufficiency by targeting SMAD, Stem Cell Res. Ther. 9 (1) (2018) 216.
[18] M. Sun, S. Wang, Y. Li, L. Yu, F. Gu, C. Wang, Y. Yao, Adipose-derived stem cells improved mouse ovary function after chemotherapy-induced ovary failure, Stem Cell Res. Ther. 4 (4) (2013) 80.
[19] C. Holmes, W. Ishida, A. Perdomo-Pantoja, B.D. Elder, E. Cottrill, J. Locke, T. F. Witham, Comparing the efficacy of adipose-derived and bone marrow-derived cells in a rat model of posterolateral lumbar fusion, J. Orthop. Res. 40 (4) (2022) 909–916.
[20] W.Z. Yang, J. Yang, L.P. Xue, L.B. Xiao, Y. Li, MiR-126 overexpression inhibits high glucose-induced migration and tube formation of rhesus macaque choroid-retinal endothelial cells by obstructing VEGFA and PIK3R2, J. Diabetes Complicat. 31 (4) (2017) 653–663.
[21] L. Mosca, A. Ilari, F. Fazi, Y.G. Assaraf, G. Colotti, Taxanes in cancer treatment: activity, chemoresistance and its overcoming, Drug Resist Updat. 54 (2021) 100742.
[22] J. Devesa, D. Caicedo, The role of growth hormone on ovarian functioning and ovarian angiogenesis, Front. Endocrinol. (Lausanne) (2019) **10**.
[23] T. Tomita, Immunohistochemical staining for lymphatic and blood vessels in normal tissues: comparison between routinely paraffin-embedded tissues and frozen sections, Acta Med. Acad. 50 (2021) 13–28.
[24] I. Akiyama, O. Yoshino, Y. Osuga, J. Shi, M. Harada, K. Koga, Y. Hirota, T. Hirata, T. Fujii, S. Saito, et al., Bone morphogenetic protein 7 increased vascular endothelial growth factor (VEGF)-a expression in human granulosa cells and VEGF receptor expression in endothelial cells, Reprod. Sci. 21 (2014) 477–482.
[25] E.J. Zaniker, E. Babayev, F.E. Duncan, Common mechanisms of physiological and pathological rupture events in biology: novel insights into mammalian ovulation and beyond, Biol. Rev. Camb. Philos. Soc. 98 (5) (2023) 1648–1667.
[26] B. Ozcelik, C. Turkyilmaz, M.T. Ozgun, I.S. Serin, C. Batukan, S. Ozdamar, A. Ozturk, Prevention of paclitaxel and cisplatin induced ovarian damage in rats by a gonadotropin-releasing hormone agonist, Fertil. Steril. 93 (5) (2010) 1609–1614.
[27] E. Aly, A.-B.I. El-Mashad, A.A. Tantawy, A.A. Amin, A comparative study on the cardiopulmonary protective effect of propolis versus coenzyme Q10 on paclitaxel-induced toxicity, J. Adv. Vet. Res. 14 (1) (2023) 59–64.
[28] M.S. Yucebilgin, M.C. Terek, A. Ozsaran, F. Akercan, O. Zekioglu, E. Isik, Y. Erhan, Effect of chemotherapy on primordial follicular reserve of rat: an animal model of premature ovarian failure and infertility, Aust. N. Z. J. Obstet. Gynaecol. 44 (1) (2004) 6–9.
[29] H. Deng, L. Zhu, Y. Zhang, L. Zheng, S. Hu, W. Zhou, T. Zhang, W. Xu, Y. Chen, H. Zhou, Q. Li, J. Wei, H. Yang, X. Lv, Differential lung protective capacity of exosomes derived from human adipose tissue, bone marrow, and umbilical cord mesenchymal stem cells in Sepsis-Induced acute lung injury, Oxid. Med. Cell Longev. 2022 (2022) 7837837.
[30] K. Dinc, R. Ozyurt, T.A. Coban, G.N. Yazici, Z. Suleyman, B. Yavuzer, et al., The effect of carvacrol on the proinflammatory cytokines, histology, and fertility outcome of cisplatin-related ovarian change in a rat model, Taiwan J. Obstet. Gynecol. 62 (2) (2023) 256–263.
[31] E. Ayazoglu Demir, A. Mentese, A. Livaoglu, N. Turkmen Alemdar, S. Demir, Ameliorative effect of gallic acid on cisplatin-induced ovarian toxicity in rats, Drug Chem. Toxicol. 46 (1) (2023) 97–103.
[32] G.O. Onder, O. Goktepe, E. Karaman, E. Karakas, O.C. Mat, D. Bolat, E. Okur, F. C. Tan, E. Balcioglu, M. Baran, M. Ermis, A. Yay, Nonylphenol exposure-Induced oocyte quality deterioration could be reversed by boric acid supplementation in rats, Biol. Trace Elem. Res. 201 (9) (2023) 4518–4529.
[33] B. Yalcin, A.H. Yay, F.C. Tan, S. Özdamar, O.G. Yildiz, Investigation of the anti-oxidative and anti-inflammatory effects of melatonin on experimental liver damage by radiation, Pathol. Res. Pract. 246 (2023) 154477.
[34] A.K. Elfayomy, S.M. Almasry, S.A. El-Tarhouny, M.A. Eldomiaty, Human umbilical cord blood-mesenchymal stem cells transplantation renovates the ovarian surface epithelium in a rat model of premature ovarian failure: possible direct and indirect effects, Tissue Cell 48 (4) (2016) 370–382.
[35] R.S. Robinson, K.J. Woad, A.J. Hammond, M. Laird, M.G. Hunter, G.E. Mann, Angiogenesis and vascular function in the ovary, Reproduction 138 (2009) 869–881.
[36] Y. Zhou, J. Zhou, X. Xu, F. Du, M. Nie, L. Hu, Y. Ma, M. Liu, S. Yu, J. Zhang, Y. Chen, Matrigel/umbilical cord-derived mesenchymal stem cells promote granulosa cell proliferation and ovarian vascularization in a mouse model of premature ovarian failure, Stem Cells Dev. 30 (2021) 782–796.
[37] M. Muta, T. Yanagawa, Y. Sai, S. Saji, E. Suzuki, T. Aruga, K. Kuroi, G. Matsumoto, M. Toi, E. Nakashima, Effect of low-dose paclitaxel and docetaxel on endothelial progenitor cells, Oncology 77 (3-4) (2009) 182–191.
[38] F. Plastino, N.A. Pesce, H. André, MicroRNAs and the HIF/VEGF axis in ocular neovascular diseases, Acta Ophthalmol. 99 (8) (2021) e1255–e1262.
[39] J. Cho, T.H. Kim, J. Seok, J.H. Jun, H. Park, M. Kweon, J.Y. Lim, G.J. Kim, Vascular remodeling by placenta-derived mesenchymal stem cells restores ovarian function in ovariectomized rat model via the VEGF pathway, Lab Invest. 101 (3) (2021) 304–317.
[40] C. Rico, A. Dodelet-Devillers, M. Paquet, M. Tsoi, E. Lapointe, P. Carmeliet, D. Boerboom, HIF1 activity in granulosa cells is required for FSH-regulated vegfa expression and follicle survival in mice, Biol. Reprod. 90 (6) (2014) 135.
[41] P. Hong, H. Yang, Y. Wu, K. Li, Z. Tang, The functions and clinical application potential of exosomes derived from adipose mesenchymal stem cells: a comprehensive review, Stem Cell Res. Ther. 10 (1) (2019) 242.
[42] H. Jang, O.H. Lee, Y. Lee, H. Yoon, E.M. Chang, M. Park, et al., Melatonin prevents cisplatin-induced primordial follicle loss via suppression of PTEN/AKT/FOXO3a pathway activation in the mouse ovary, J. Pineal Res. 60 (3) (2016) 336–347.
[43] D. Dewailly, J. Laven, AMH as the primary marker for fertility, Eur. J. Endocrinol. 181 (6) (2019) D45–D51.
[44] M.J. Gruijters, J.A. Visser, A.L. Durlinger, A.P. Themmen, Anti-mullerian hormone and its role in ovarian function, Mol. Cell Endocrinol. 211 (1-2) (2003) 85–90.
[45] G. Courtois, A. Smahi, NF-kappaB-related genetic diseases, Cell Death Differ. 13 (5) (2006) 843–851.
[46] F. Benzer, F.M. Kandemir, S. Kucukler, S. Comaklı, C. Caglayan, Chemoprotective effects of curcumin on doxorubicin-induced nephrotoxicity in wistar rats: by modulating inflammatory cytokines, apoptosis, oxidative stress and oxidative DNA damage, Arch. Physiol. Biochem. 124 (5) (2018) 448–457.
[47] A. Yardım, F.M. Kandemir, S. Çomaklı, S. Özdemir, C. Caglayan, S. Kucukler, H. Çelik, Protective effects of curcumin against paclitaxel-induced spinal cord and sciatic nerve injuries in rats, Neurochem. Res. 46 (2) (2021) 379–395.
[48] A.G. Ramadan, W.M. Abdel-Rehim, R.A. El-Tahan, S.S. Elblehi, M.A. Kamel, S. A. Shaker, Maternal and paternal obesity differentially reprogram the ovarian mitochondrial biogenesis of F1 female rats, Sci. Rep. 13 (1) (2023) 15480.
[49] C.E. Aiken, J.L. Tarry-Adkins, N.C. Penfold, L. Dearden, S.E. Ozanne, Decreased ovarian reserve, dysregulation of mitochondrial biogenesis, and increased lipid peroxidation in female mouse offspring exposed to an obesogenic maternal diet, FASEB J. 30 (4) (2016) 1548–1556.
[50] M.V. Bazzano, A. Köninger, M.E. Solano, Beyond defence: immune architects of ovarian health and disease, Semin. Immunopathol. 46 (3-4) (2024) 11.
[51] J. Liu, T. Chen, P. Lei, X. Tang, P. Huang, Exosomes released by bone marrow mesenchymal stem cells attenuate lung injury induced by intestinal ischemia reperfusion via the TLR4/NF-κB pathway, Int. J. Med. Sci. 16 (9) (2019) 1238–1244.
[52] J.S. Heo, Y. Choi, H.O. Kim, Adipose-derived mesenchymal stem cells promote M2 macrophage phenotype through exosomes, Stem Cells Int. 2019 (2019) 7921760.